Crystalline Tubes of Myosin Subfragment-2 Showing the Coiled-Coil and Molecular Interaction Geometry

Roy A. Quinlan and Murray Stewart

Medical Research Council, Laboratory of Molecular Biology, Cambridge CB2 2QH, England

Abstract. We have produced crystalline tubes of chicken breast myosin long subfragment-2 that show order to resolutions better than 2 nm. The tubes were formed from a thin sheet in which the myosin long subfragment-2 molecules were arranged on an approximately rectangular crystalline lattice with a = 14.1 ± 0.2 nm and b = 3.9 ± 0.1 nm in projection. Shadowing indicated that the tube wall was ~7 nm thick and that the sheets from which it was formed followed a right-handed helix. Superposition of the lattices from the top and bottom of the tube produced a moire pattern in negatively stained material, but images of single sheets were easily obtained by computer image processing. Although several molecules were superimposed perpendicular to the plane of the sheet, the modulation in density due to the coiled-coil envelope was clear, indicating that the coiled-coils in these molecules were in register (or staggered by an even number of quarter pitches). In projection the coiled-coil had an apparent pitch of 14.1 nm (the axial repeat of the unit cell), but the small number of molecules (probably four) superimposed perpendicular to the plane of the sheet meant that pitches within ~1 nm of this value could have shown a modulation. Therefore, a more precise determination of the coiled-coil pitch must await determination of the sheet's three-dimensional structure. The coiled-coils of adjacent molecules within the plane of the sheet were staggered by an odd number of quarter pitches. This arrangement was similar to that between paramyosin molecules in molluscan thick filaments and may have features in common with other coiled-coil protein assemblies, such as intermediate filaments. Each molecule in the crystal had two types of neighbor: one staggered by an odd number of quarter pitches and the other by an even number of quarter pitches, as has been proposed for the general packing of coiled-coils (Longley, W., 1975, *J. Mol. Biol.*, 93:111–115). We propose a model for the detailed packing within the sheet whereby molecules are inclined slightly to the plane of the sheet so that its thickness is determined by the molecular length.

MYOSIN is an important component of muscle and many other motile systems where it usually associates into "thick" filaments that interact with "thin" actin-containing filaments to generate movement and force. The myosin molecule contains two heavy chains and four light chains and has an M_r of ~450,000. Morphologically, the molecule is composed of two globular heads that interact with actin, and a long fibrous tail, part of which assembles into the thick filament shaft (reviewed by Harrington and Rodgers, 1985). The arrangement of myosin heads on the surface of relaxed thick filaments has been determined for a number of species (Castelanni, et al., 1983; Crowther, et al., 1985; Kensler and Stewart, 1983, 1986; Vibert and Craig, 1983; Stewart and Kensler, 1986; Stewart, et al., 1981*b*, 1985*b*). However, the detailed packing of the myosin tails in the thick filament shaft has yet to be determined, although some aspects of the molecular packing of paramyosin that forms the core of a number of invertebrate muscle thick filaments have been established (Elliott and Bennett, 1984). Moreover, in many nonmuscle systems the assembly of myosin appears to be a dynamic process that may play a role in the regulation of motility. It is therefore important to establish the structure of the tail portion of myosin and the molecular basis of the interactions in myosin-containing filaments.

Proteolysis of myosin yields a number of fragments that retain part of the physiological function of the molecule (reviewed by Harrington and Rodgers, 1985). Thus, papain or chymotryptic digestion gives isolated heads that are soluble under physiological buffer conditions and that contain an actin-activated ATPase, and the rod or tail section of the molecule that aggregates under physiological conditions. Further proteolysis of the rod yields light meromyosin (LMM),[1] which contains the COOH-terminus of the heavy chain and which constitutes the portion of the tail distal to the heads; and long subfragment-2 (long S-2), which links LMM to the heads (Weeds and Pope, 1977). Under physiological buffer conditions, LMM is insoluble and is broadly thought to cor-

1. *Abbreviations used in this paper*: LMM, light meromyosin; long S-2, long subfragment-2; short S-2, short subfragment-2.

respond to the portion of the rod that is bound in the thick filament shaft. On the other hand, long S-2 is soluble in these conditions and is thought to correspond to the portion of the rod that forms part of the cross-bridge in rigor and contracting muscle and which links the actin-binding heads to the thick filament shaft (reviewed by Harrington and Rodgers, 1985). Further proteolysis of long S-2 yields a smaller fragment referred to as short subfragment-2 (short S-2). LMM, long S-2, and short S-2 have relative molecular mass values of about 75,000, 56,000, and 35,000, respectively (Weeds and Pope, 1977; Stewart and Edwards, 1984; Sutoh, et al., 1978).

The rod portion of the myosin molecule has a coiled-coil conformation (reviewed by Fraser and MacRae, 1973; Cohen and Parry, 1986) in which two α-helical chains are wound in a left-handed helix with a pitch of ~14–20 nm. The two chains are in register (Stewart, 1982) and parallel, and are thought to be stabilized by extensive hydrophobic interactions (see Crick, 1953; Fraser and MacRae, 1973; Cohen and Parry, 1986). The coiled-coil has a diameter of ~2 nm (Fraser and MacRae, 1973) and seems similar to that found in tropomyosin, paramyosin, α-keratins, and intermediate filament proteins. Detailed mathematical analysis of rod sequences has demonstrated the presence along the rod of a periodically varying distribution of charge that repeats every 28 residues (McLachlan and Karn, 1982, 1983; Parry, 1981). It seems very likely that myosin rods associate so that the charge pattern in one molecule is complemented by adjacent molecules, which would happen if molecules were staggered by an odd multiple of 14 residues (McLachlan and Karn, 1982, 1983; Parry, 1981).

Although there have been a number of studies of the aggregates produced from LMM or rod under a range of conditions (Bennett, 1976; 1981; Chowrashi and Pepe, 1977; Katsura and Noda, 1973; Safer and Pepe, 1979; Yagi and Offer, 1981), none of these aggregates have been sufficiently well ordered to yield high resolution information by electron microscopy or x-ray diffraction. Therefore, although some aspects of the axial positioning of molecules have been established, it has not been possible to visualize the coiled-coil and to study the molecular basis of the interactions between myosin rods or LMM. In comparison, aggregates from long S-2 have not been investigated so extensively, although Ueno et al. (1983) did report the formation of ordered aggregates of rabbit long S-2 in the presence of magnesium ions. In this paper we extend this work in two ways. First, we show that under appropriate conditions, chicken breast myosin gives a very homogeneous and stable preparation of long S-2. Second, we show that this material gives highly ordered aggregates that are suitable for investigation at resolutions better than 2 nm by electron microscopy. Furthermore, reconstructed images of this material enable the density modulation due to the molecular coiled-coils to be observed and also establish some aspects of the geometry of interaction between molecules.

Materials and Methods

Production of Long S-2 and Aggregate

Myosin was prepared from chicken breast muscle as described by Weeds and Pope (1977) and was used either fresh or after storage in 50% glycerol at −20°C. Rod was prepared from whole myosin at ~15 g/liter in 0.2 M ammonium acetate, 2 mM Ca acetate, 1 mM dithiothreitol (DTT), pH 7, at 20°C, by digestion with papain (24 U/mg, type III; Sigma Chemical Co., St. Louis, MO) at an enzyme/substrate ratio of 1:1000 for 3 h. Digestion was terminated by addition of 3 mM iodoactetic acid (Sigma Chemical Co.). After 10 min, DTT was added to 1 mM to remove excess alkylating agent. Under the conditions employed, the rod formed a dense precipitate which was collected by centrifugation at 10,000 *g*. The material obtained in this way was essentially homogeneous and was used to produce long S-2 without further purification. When necessary, rod was stored frozen at −20°C.

To produce long S-2, rod was dissolved in 1 M ammonium acetate, 2 mM Ca acetate, 1 mM DTT, pH 7, at 20°C, at ~30 g/liter and dialyzed exhaustively against 0.5 M ammonium acetate, 2 mM Ca acetate, 1 mM DTT, pH 7, at 4°C. The rod solution was then diluted with dialysate to a final rod concentration of 15 g/liter, taking the extinction coefficient of rod (1% at 280 nm) as 0.3 (Weeds and Pope, 1977). Chymotrypsin (65 U/mg Millipore Corp., Bedford, MA) was then added to a concentration of 0.075 g/liter. The digestion was monitored by one-dimensional SDS-PAGE and was terminated by the addition of PMSF (phenylmethylsulfonyl fluoride) to a concentration of 1 mM when digestion of the rod was essentially complete. Typically digestion times of ~45 min were used (see Fig. 1). The principal products of the digest were long S-2 and LMM, and the latter was removed, after dialyzing to 0.1 M ammonium acetate, by centrifugation at 10,000 *g* at 4°C. The supernatant, which contained almost homogeneous long S-2 and a little undigested rod, was either lyophylized or dialyzed against 10 mM Na phosphate, 50 mM NaCl, pH 6.2, at 4°C.

The long S-2 was further purified by ammonium sulphate fractionation between 40 and 55% saturation in 50 mM NaCl, 10 mM Na phosphate buffer, pH 6.2, at 4°C. The precipitate was dissolved in 1 M ammonium acetate, 1 mM DTT, pH 7, at 4°C and dialyzed exhaustively against 0.1 M ammonium acetate, 1 mM DTT, pH 7, at 4°C. The resultant solution was stored frozen at −20°C until required. Repeated freezing and thawing did not appear to influence the ability of preparations to produce crystalline aggregates under defined conditions.

Crystalline tubes were formed by dialyzing ~10 g/liter long S-2 in 1.5 M NaCl, 0.1 M ammonium acetate, 1 mM DTT, pH 7, at 4°C against 20 mM NaCl, 30 mM $MgCl_2$, 1 mM DTT, 30 mM imidazole-HCl, pH 6.65 at 4°C. To ensure a slow change of solution composition, the dialysis sack containing the long S-2 solution was placed inside a second sack that contained ~25 vol of sample buffer. This second sack was then placed in a large volume of the dialysate. The major dialysate solution was changed after 24 h. In some instances 30 mM $CaCl_2$ or 30 mM $SrCl_2$ was substituted for $MgCl_2$ and seemed to produce analogous crystalline tubes.

SDS-PAGE was as described by Laemmli (1970) using 6–15% gradient gels.

Electron Microscopy and Diffraction

Specimens for electron microscopy and electron diffraction were absorbed onto thin carbon films, either directly on grids or using the method of Valentine et al. (1968), and then washed with water or negatively stained with 1% unbuffered aqueous uranyl acetate before air drying. Positively stained tubes were prepared by washing with approximately 10 drops of demineralized water after staining with uranyl acetate. Generally, preservation was improved by including ~0.1% isoamyl alcohol in the last solution before drying. Some samples were fixed by positive staining with uranyl acetate (Kensler and Stewart, 1983; 1986), freeze-dried, and shadowed with platinum in a Balzers BA 300 freeze-fracture apparatus at nominal angles of 10 or 20°. Tobacco mosaic virus (generously provided by Dr. P. J. G. Butler of this laboratory) was used to calibrate the shadowing angle, taking the diameter of the particles as 18 nm (Namba and Stubbs, 1986). Molecular lengths were determined from preparations sprayed onto mica and unidirectionally shadowed at 10° with platinum as previously described (Stewart and Edwards, 1984).

Material was examined at 80 kV with a Philips EM420 electron microscope using a 0.03-mm objective aperture and standard imaging conditions. Micrographs were recorded on Kodak SO-163 cut film, generally at nominal magnifications near 50,000 for negatively and positively stained material and 20,000 for shadowed material. Magnification was calibrated with a shadowed replica of a 2160 lines/mm optical diffraction grating. Selected area electron diffraction patterns were recorded using a 0.01-mm diffraction aperture and camera lengths of 0.14–0.45 m for high angle reflections such as the 0.51 nm, and 1–2.5 m for low angle reflections.

Indexing of Diffraction Patterns

Optical diffraction patterns from electron micrographs (Fig. 5) and low angle electron diffraction patterns (Fig. 6) from negatively stained material

showed a distinctive pattern of spots characteristic of overlapping lattices from the sheets corresponding to the top and bottom of the collapsed tubes. As illustrated in Fig. 7, the pattern from a single sheet was easily indexed on an approximately rectangular lattice. The sheet from which the tubes were formed appeared to have either *pg* or *pmg* symmetry (see Henry and Lonsdale, 1969) as evidenced by the absence of an equatorial (1, 0) reflection at 3.9 nm (Figs. 5, 6, and 7). However, the lattice appeared to have been slightly distorted (by ~4°) on winding into the tube, so that the lattice was no longer exactly rectangular. Formally, therefore, the lattice must have either *p1* or *p2* symmetry, and so in subsequent image processing no averaging of data based on higher symmetry was undertaken. However, because the distortion of the lattice from rectangular was very slight, it seemed natural to discuss the structure in terms of the rectangular lattice and also to index the spots accordingly. Patterns in all figures are oriented so that the molecule axis is vertical and so the tube axis is horizontal. Therefore, equatorial reflections derive from spacings perpendicular to the molecular axis and meridional reflections derive from spacings along the molecule.

It was not possible to decide unequivocally whether the rectangular lattice had *pg* or *pmg* symmetry, as there were too few reflections of sufficient strength to enable accurate amplitudes and phases to be determined. As illustrated in Table I, at low resolution the pattern certainly had features characteristic of *pmg* symmetry, but it was not clear whether this was so at higher resolution. The phase of the 0,7 reflection did not appear to be consistent with *pmg* symmetry, and the clear difference in intensity between the 2,1 and 2,−1 reflections (see Fig. 6) was similarly not consistent with the higher symmetry. Furthermore, there were some indications (see Discussion, first section) that the molecules within a sheet might be polar, which would imply *pg* symmetry. As the positive staining pattern of the material was so weak, it was not possible to establish this feature of the structure definitively. Because of these uncertainties, it was thought prudent to assume only the minimum symmetry consistent with the data when undertaking Fourier-based image processing.

Image Processing

Electron micrographs were initially assessed by optical diffraction to select areas in which the structure was well preserved, the defocus was optimal (~200–500 nm under focus), and astigmatism was negligible. These regions were digitized at spacings corresponding to ~0.4 nm on the original object and Fourier transforms computed from areas containing 1,024 × 1,024 picture elements. The moire pattern produced by the superposition of the lattices from the top and bottom of the flattened tube was decomposed into its constituent halves by Fourier-based filtering (for reviews, see Aebi et al., 1984; Stewart, 1986). This method relied on separating, in the Fourier transform, the contributions at the top of the tube from those at the bottom. As illustrated in Fig. 7, the lattice of each was easily identified and reflections corresponding to a single side could be assigned with confidence. The diffuse nature of the lattice points (particularly the 2,0 reflection) indicated there was some disorder in the specimens, and so the signal to noise ratio was enhanced by integrating around each lattice point as previously described (Stewart and Beveridge, 1980). Data from six sets of reflections (three top and three bottom) were averaged and are shown in Table I. Reconstructed images were produced from these data by Fourier inversion and displayed on raster graphics device (767; AED, Inc., Sunnyvale, CA) using standard image processing software derived, with many improvements, from DeRosier and Moore (1970).

Results

Digestion of Chicken Rod and Production of Aggregates

Minor modification of the protocols usually used to produce long S-2 by digestion of myosin rod gave a substantially more homogeneous product and appeared to markedly reduce the amount of concurrent digestion of the long S-2 produced to short S-2. By optimizing the composition of the digestion buffer, and particularly by eliminating chloride ion as suggested by the work of Stafford (1985), the stability of long S-2 seemed to be markedly increased so that it was possible to digest rod almost to completion as shown by the time course of digestion in Fig. 1. This digestion behavior contrasted

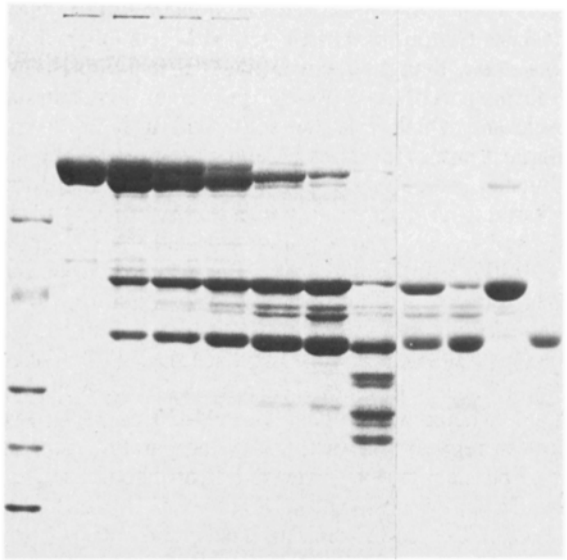

Figure 1. SDS-PAGE analysis of the time course of digestion of chicken breast myosin rod with chymotrypsin. (Lane *a*) M_r standards; (lane *b*) starting material; (lanes *c–g*) samples taken after 5, 10, 15, 30, and 60 min, respectively; (lane *h*) sample after digestion for 16 h. Under the conditions used, the digestion yielded primarily two bands: LMM at M_r 75,000, and long S-2 at M_r 56,000. In contrast to previous protocols, there was little subsequent digestion of long S-2 to short S-2, even when digestion was taken almost to completion (lane *g*). Furthermore, even after severe overdigestion (lane *h*), there was still a substantial quantity of long S-2 present. Lane *i* shows material digested for 45 min that was used for bulk preparation of long S-2. This material contained mainly LMM and long S-2, with a little undigested rod. The LMM was removed by centrifugation (lane *j*) and other contaminants by ammonium sulphate fractionation (lane *k*) to leave essentially homogeneous long S-2 (lane *l*).

with previous preparative protocols (Sutoh et al., 1978; Stewart and Edwards, 1984) in which only a limited digest was possible and where it was generally necessary to chromatographically separate the resultant mixture of long and short S-2. It is likely that the high homogeneity of the long S-2 we produced was a factor in the production of crystalline aggregates of high order. The molecular length of this material, determined by low angle shadowing, was 61 ± 6 nm (±SD, n = 50), similar to that found by other workers for rabbit long S-2 of similar relative molecular mass (Stewart and Edwards, 1984; Walzthony et al., 1986). Thus, it seemed unlikely that under our protocol cleavage had occurred at a radically different position in the chicken myosin rod.

We explored a broad range of precipitation conditions in a search for crystalline aggregates of long S-2 and found that crystalline tubes (evidenced in the solution only by a slight turbidity) were formed between pH 6 and 7.75 in the presence of 30 mM magnesium ions. Similar aggregates were formed in the presence of calcium and strontium ions or of spermidine, but not in the presence of barium. Precipitates formed in the absence of high divalent cation concentration or at other pH values were generally either amorphous or paracrystalline, as assessed by electron microscopy of negatively stained material.

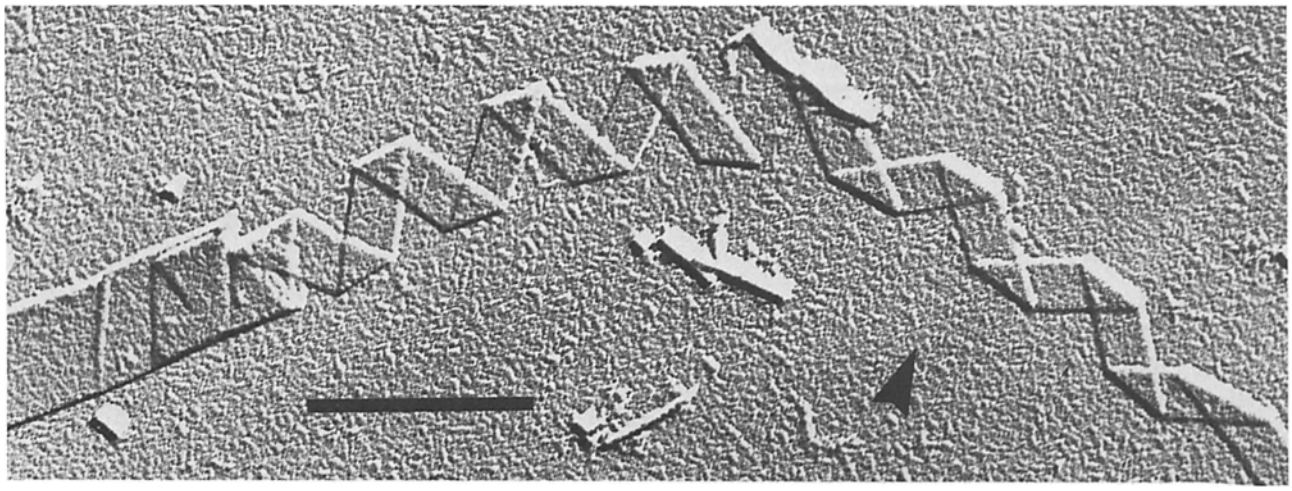

Figure 2. Tube of long S-2 fixed with uranyl acetate and shadowed unidirectionally with platinum at a nominal angle of 10°. Tobacco mosaic virus has been included to calibrate thickness measurements. Note how the tube has been formed by a sheet rolling up in a right-handed helical manner. Arrow shows shadow direction. Bar, 1,000 nm.

General Appearance of the Aggregates

Low magnification views of negatively stained or shadowed material (Figs. 2, 3, and 4) showed the presence of tubes that, in many instances, could be seen to have been formed by a thin sheet rolling up. The tubes were generally ~600 nm wide, after being flattened onto the grid, which would correspond to a diameter of ~400 nm, whereas the sheet from which they were formed was generally ~200–300-nm wide. Material shadowed at a nominal angle of 10° (Fig. 2) indicated that the flattened tube was 14.1 ± 1.5 nm (±SD, n = 17) thick, whereas the sheets from which they were constructed were 7.2 ± 1.0 nm (±SD, n = 12) thick. (In addition to random errors, there may also have been systematic errors of the order of 1 to 2 nm in the data derived from shadowed

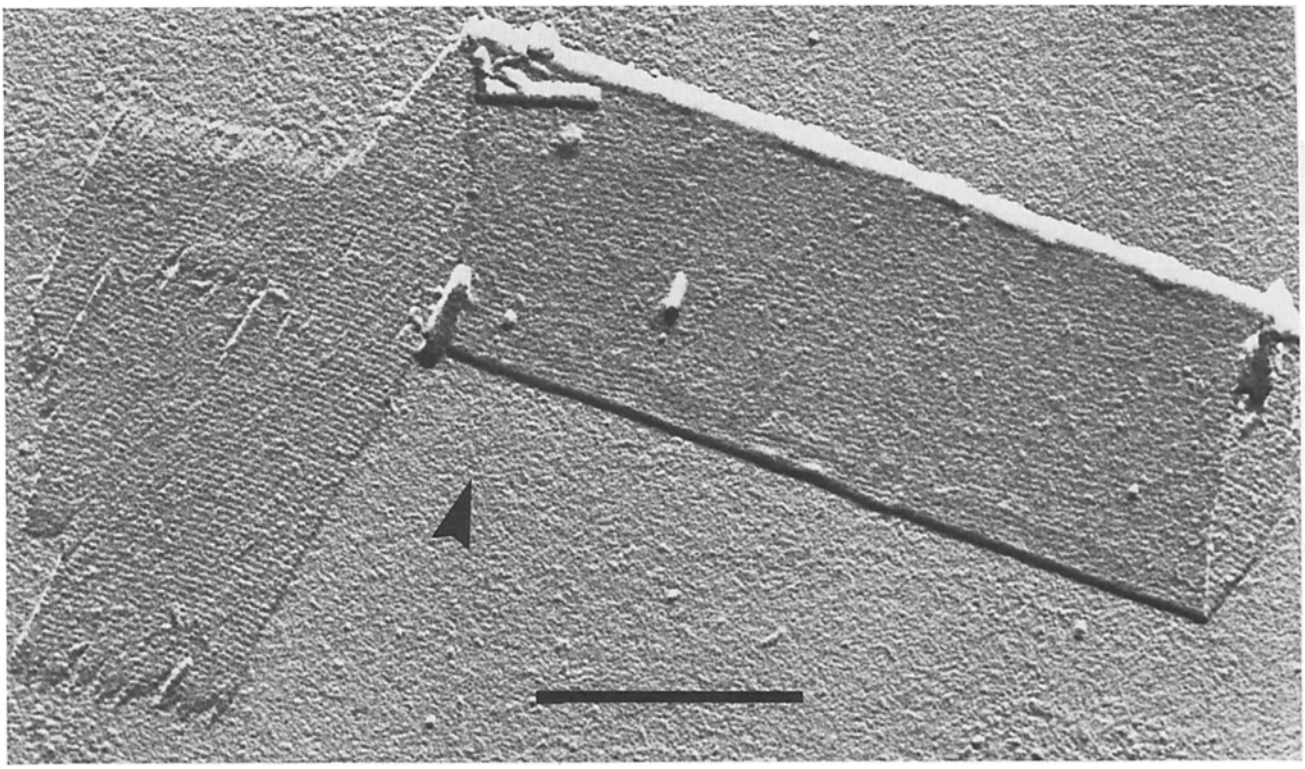

Figure 3. Tube of long S-2 fixed with uranyl acetate and shadowed unidirectionally with platinum at a nominal angle of 20°. This highlighted a series of striations on both inner and outer surfaces of the tube that were aligned almost parallel to the tube axis and so perpendicular to the molecular direction. The spacing between bands was ~14 nm and they probably resulted from molecular ends protruding from the surface of the sheet. Arrow indicates direction of shadowing. Bar, 500 nm.

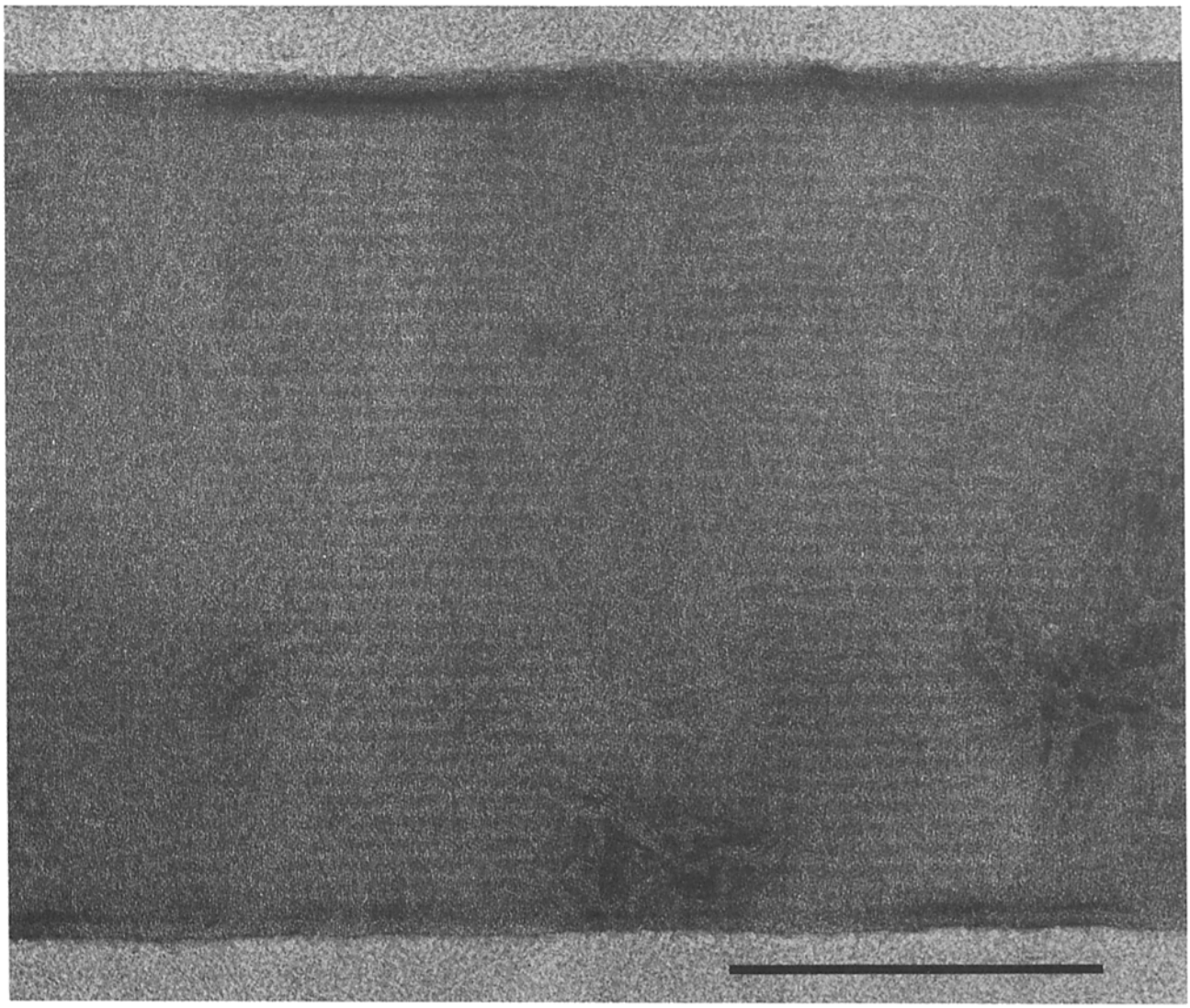

Figure 4. High magnification electron micrograph of a negatively stained long S-2 tube showing the moire pattern resulting from the superposition of patterns from the top and bottom of the tube. This makes direct interpretation of molecular positions and interactions difficult. Tube axis is horizontal. Bar, 250 nm.

material as a result of accumulation of metal and other artefacts. Consequently, the absolute value of the sheet thickness determined in this way may be slightly in error.) Since a single coiled-coil is ~2 nm in diameter (Fraser and MacRae, 1973), this indicated that probably four molecules were stacked in a direction roughly perpendicular to the plane of the sheet. The shadowed images indicated that the sheet was wound into tubes in a right-handed helical manner (Figs. 2 and 3). In addition, there was a feint pattern of striations perpendicular to the sheet axis (and so nearly parallel to the axis of the tube) and spaced ~14 nm apart on each surface of the sheet that made up the tube. This was more easily seen on material shadowed at a nominal angle of 20° (Fig. 3). Fine detail was obscured in high magnification images of negatively stained material (Fig. 4) as a result of a moire pattern formed by superposition of information from the top and bottom of the tube. There was also a feint axial striation seen in these images that probably derived from superposition of the 14-nm surface repeats seen in shadowed images (Fig. 3).

Image Analysis

Optical diffraction (Fig. 5) and low angle electron diffraction (Fig. 6) patterns showed pairs of very strong equatorial reflections at 1.95 nm that indicated that substructure had been well preserved in negatively stained material. Overall, the appearance of the patterns obtained with characteristic pairs of spots was that expected from the moire pattern produced by the overlying sheets from the top and bottom of the tube (e.g., Brisson and Unwin, 1984; Stewart, 1986; Yanagida et al., 1972). As shown in Fig. 7, the pattern was easily indexed and a single sheet had a near-rectangular lattice with $a = 14 \pm 0.2$ nm ($\pm$SD, $n = 23$), $b = 3.9 \pm 0.1$ nm ($\pm$SD, $n = 23$) and $\gamma = 94 \pm 2°$ ($\pm$SD, $n = 6$). The slight departure of the angle between the axes from 90° probably reflected the slight distortion of the sheet produced by winding into a tube. The strong 1.95-nm reflection corresponds to the diameter of a coiled-coil (see Fraser and MacRae, 1973) and indicated that the long S-2 molecules were arranged almost perpendicular to the axis of the tube. High an-

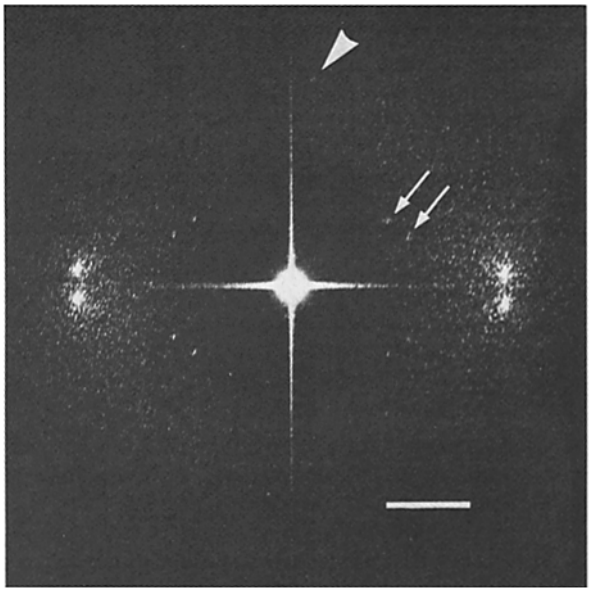

Figure 5. Optical diffraction pattern from the negatively stained long S-2 tube illustrated in Fig. 4. There are very strong equatorial reflections at 1.95 nm, indicating a high degree of structural preservation. In addition the pattern shows a number of weaker spots that can be indexed on two overlapping lattices corresponding to the top and bottom of the flattened tube (see Fig. 7). Arrows show the off-axis pairs of spots that are analogous to those seen in low angle x-ray diffraction patterns (see text) and which probably derive from the coiled-coil. Arrowheads show the 0,7 axial reflections (see Fig. 7). The pairing of spots seen in this pattern is characteristic of a superposition moire pattern produced by two lattices rotated relative to one another. The pattern is oriented to correspond to the tube axis being horizontal. Bar, 1/(5 nm).

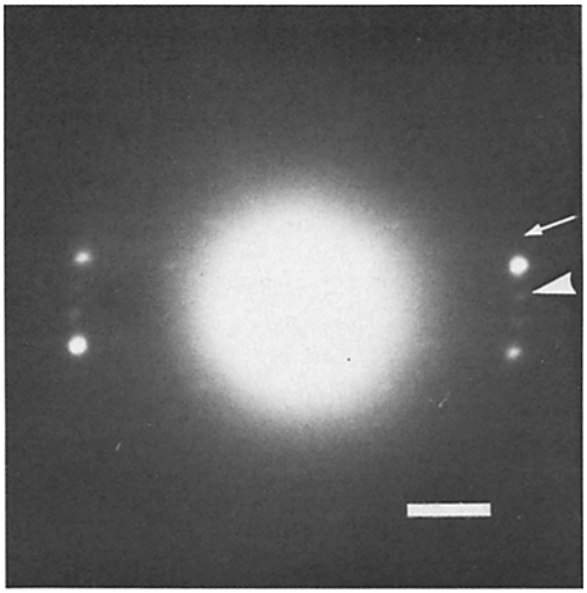

Figure 6. Low angle electron diffraction pattern of a negatively stained tube. The equatorial reflections at 1.95 nm are easily seen, but the inner reflections on the 3.9-nm row line are partially obscured by the rapidly varying background produced by inelastically scattered electrons. Note the marked difference in intensity between the 2,1 reflection (see Fig. 7), which is clearly seen (*arrowhead*), and the 2,−1 reflection, which is too weak to be seen on the print (*arrow*). The angle between the superimposed lattices in this example is different than that seen in Fig. 5. Patterns such as this were useful in identifying well preserved areas for imaging and were also used to measure the angle between lattices in the top and bottom of tubes. The preservation of this tube was somewhat better on its upper surface and so the series of reflections deriving from the top (see Fig. 7) were stronger than those deriving from the bottom. Patterns such as this were therefore also useful in confirming the indexing illustrated in Fig. 7. The pattern is oriented to correspond to the tube axis being horizontal. Bar, 1/(5 nm).

gle electron diffraction patterns confirmed this molecular orientation. As shown in Fig. 8, these patterns showed a sharp unsampled arc at 0.51 nm, oriented approximately perpendicular to the tube axis, which derived from the α-helical pitch, and also a diffuse 1 nm equatorial reflection, weakly sampled by the 3.9-nm repeat, characteristic of α-helices (Cohen and Holmes, 1963; Fraser and MacRae, 1973).

The precise angle between the molecules in the top and bottom of the tube tended to vary between specimens and, as illustrated in Fig. 9, there seemed to be a number of preferred orientations separated by intervals of ~4°, with ~23° seeming most common. This effect was probably a result of different tube diameters (quantized on the circumferential translation between long S-2 molecules in the tubes) and different sheet widths (quantized on the molecular diameter). Each step of ~4° would correspond to a shift of only a few angstrom units between adjacent molecules, and so it would seem unlikely that this was reflecting a series of different molecular interaction geometries.

In addition to the 1.95-nm equatorial reflection, optical diffraction patterns showed off-axis reflections that indexed as the 1,2 and 1,−2 orders of an approximately rectangular lattice. These off-axis reflections were generally absent from low angle electron diffraction patterns and from optical diffraction patterns (Fig. 11) of positively stained specimens (Fig. 10), which showed only weak 1.95-nm equatorial reflections. The appearance of the positively stained patterns indicated that the structure seen in negatively stained material was due primarily to the stain outlining the envelope of the molecule and not to specific attachment of stain to particular residues of the molecule as seen, for example, in tropomyosin (Caspar et al., 1969; Stewart, 1981, 1984). These off-axis reflections were spaced at 3.9 nm radially (that is, along the equator) and 7.2 nm axially (along the meridian), and were in some ways analogous to the diffuse reflections seen in low angle x-ray diffraction patterns of molluscan muscle (Cohen and Holmes, 1963; Elliot and Bennett, 1984; Elliott and Lowy, 1970; Elliott et al., 1968) at a similar axial spacing. (Because of the three-dimensional nature of the unit cell in the molluscan filaments, the radial spacing of the corresponding off-axis reflections was $1/\sqrt{2}$ the spacing of the equatorial maximum or at ~2.8 nm). These off-axis reflections in x-ray diffraction patterns are thought to probably derive from sampling of the second layer line corresponding to the long-pitch helix of the molecular coiled-coil. In contrast to the off-axial reflections, the corresponding equatorial reflection at 3.9 nm was conspicuously absent in our optical and electron diffraction patterns, indicating that it was forbidden by the symmetry of the sheet. This implied that there was a glide plane parallel to the direction of the molecules' axes and so alternate molecules across the sheet

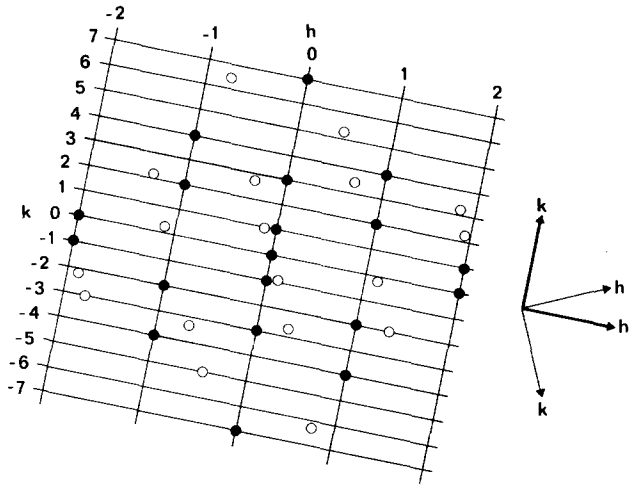

Figure 7. Illustration of how the diffraction patterns shown in Figs. 5 and 6 can be indexed in terms of two nearly rectangular lattices, each deriving from a single sheet. Spots deriving from the sheet corresponding to the top of the tube are shown as full circles and those deriving from the bottom sheet as open circles. Both patterns correspond to a unit cell with a = 14.1 nm and b = 3.9 nm. The lattice for the top has been indicated, together with the Miller indices (h and k) corresponding to the spots. Note the characteristic absence of an equatorial (1,0) reflection at 3.9 nm, which indicated that in projection adjacent molecules were staggered. The patterns are oriented to correspond to the tube axis horizontal. Arrows to the *right* of the figure indicate the direction of the lattice vectors for the top (*bold arrows*) and bottom (*light arrows*) of the sheet.

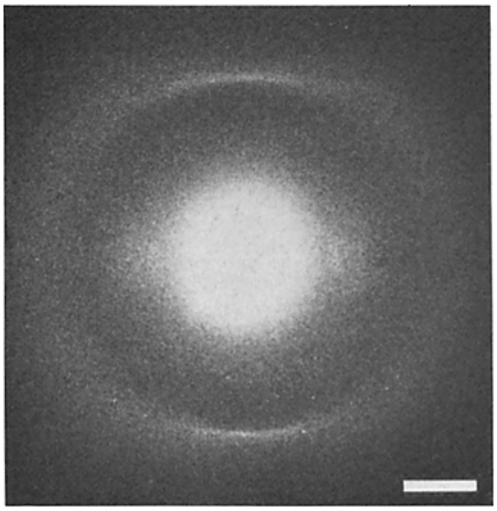

Figure 8. High angle electron diffraction pattern from negatively stained material oriented to correspond to the tube axis being horizontal. There is a sharp, unsampled meridional arc at 0.51 nm and a diffuse equatorial reflection at 1 nm that is weakly sampled by the 3.9-nm equatorial repeat. These two reflections are characteristic of an α-helical structure arranged with its axis vertical, or perpendicular to the tube axis. This confirms the molecular orientation deduced from the low angle optical and electron diffraction patterns (Figs. 5–7). The large, diffuse central density was due to inelastically scattered electrons. Bar, 1/(2 nm).

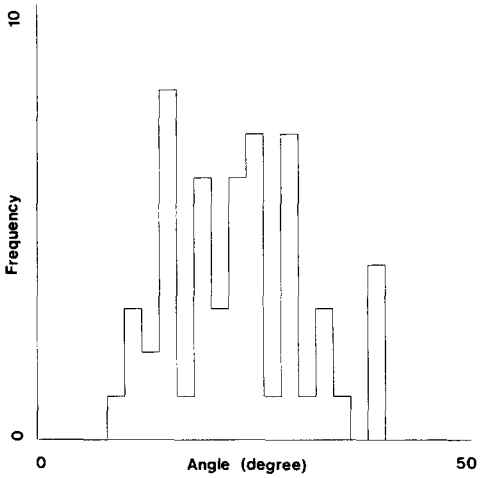

Figure 9. Distribution of angles between molecules in the top and bottom of negatively stained tubes of long S-2 determined by measuring the angular separation between the corresponding 1.95-nm reflections in low angle electron diffraction patterns. There appeared to be a series of preferred orientations separated by intervals of ~4–5°.

were staggered axially by half a repeat. Low angle x-ray diffraction patterns of molluscan muscle similarly lack an analogous equatorial reflection (Elliott and Bennett, 1984; Elliott and Lowy, 1970; Elliott et al., 1968).

The moire pattern formed between the top and bottom of the tube (Fig. 4) made it impossible to interpret directly the high degree of structural information that optical diffraction indicated was present in the micrographs. We therefore used computer image processing to obtain an image of one side of the tube (i.e., of a single sheet). This was possible because the signal from the top and bottom of the tube could be separated in the Fourier transform of the object (see Fig. 7) and this enabled an image of a single side to be reconstructed by Fourier inversion (see, for example, Brisson and Unwin, 1984; Klug and DeRosier, 1966; Stewart, 1986; Stewart et al., 1985*a*; Yanagida et al., 1972). Six sets of reflections corresponding to a single side were averaged (see Table I) and had a root mean square amplitude residual of 19% and an amplitude-weighted phase residual of 18°. Reconstructed images of single sheets (Fig. 12) showed a distinctive pattern of rods that we interpret as several (probably four) molecules superimposed in the direction of view. There was a clear density modulation along each rod, which we interpret as arising from the long S-2 coiled-coil viewed in projection as illustrated in Fig. 13. This modulation indicated that the coiled-coil pitch was close to the sheet axial repeat of 14.1 nm. Because several (probably four) molecules were superimposed in this projection of the structure, the clarity of the coiled-coil modulation indicated that successive molecules in a direction perpendicular to the plane of the tube had their coiled-coils in register, or at least nearly so. If the coiled-coils were perfectly in register, then their pitch would be 14.1 nm. However, because only a small number of molecules were superimposed in a direction perpendicular to the plane of the sheet, it was possible that the coiled-coil pitch could have had a value slightly different than the axial repeat of the crystal. Because successive molecules must be staggered by an integer multiple (probably 1) of 14.1 nm axially, a coiled-coil pitch near 14.1 nm would still give a density modulation with a period of 14.1 nm. However, in these cir-

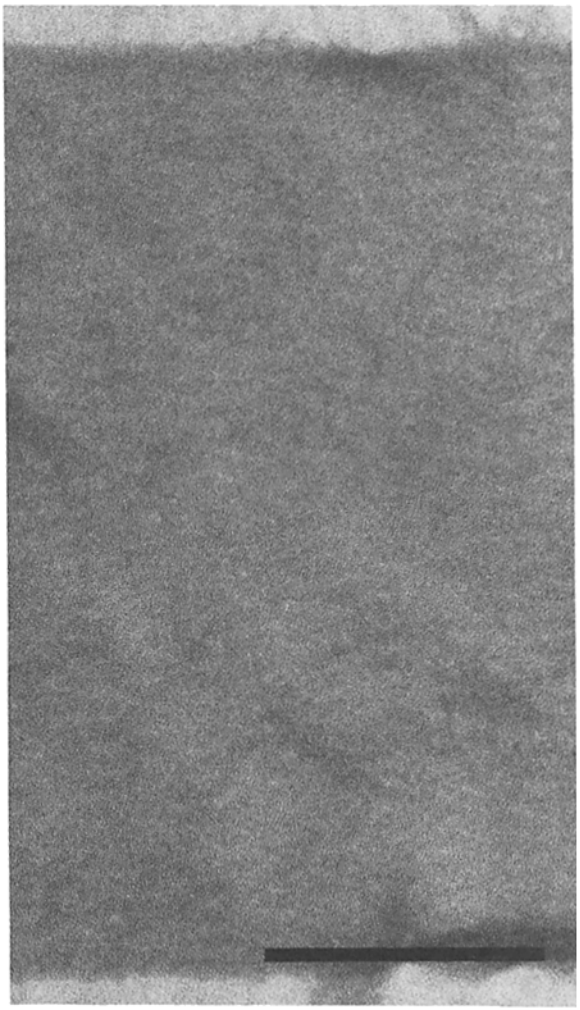

Figure 10. Electron micrograph of a long S-2 tube positively stained with uranyl acetate. Compared with negatively stained images (Fig. 4) the pattern is rather faint and most of the fine structure has been lost, although a 14-nm banding parallel to the tube axis can still be made out. Bar, 150 nm.

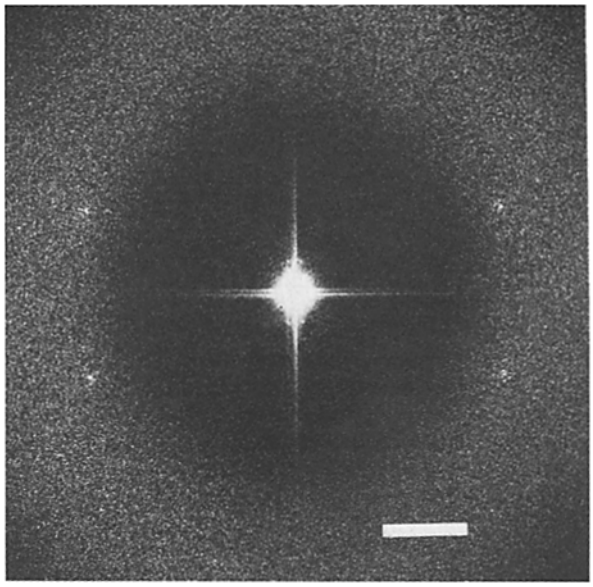

Figure 11. Optical diffraction pattern from the positively stained tube shown in Fig. 10. The pattern is weak compared with diffraction patterns from negatively stained material (Fig. 5); only very weak (2,0) reflections could be seen at 1.95 nm and the 1,2 and 1,−2 reflections on the 3.9-nm row line were absent. This indicated that the pattern in the negatively stained material derived primarily from the stain delineating the molecular envelope rather than from specific attachment of the stain to particular residues along the long S-2 molecule. Bar, 1/(5 nm).

cumstances, the coiled-coils of successive molecules in a direction perpendicular to the plane of the sheet would not be perfectly in register; they would get progressively out of register and so, in a crystal of infinite thickness, would interfere so that there was no net modulation in projection. However, when only a small number of molecules are superimposed, the interference will not be complete if the mismatch between coiled-coil pitch and axial translation is not large. Thus, coiled-coil pitches within ~1 nm of 14.1 nm were probably consistent with the pattern we observed in projection. A more precise value of the coiled-coil pitch must await solution of the structure of the sheets in three dimensions, which we are presently undertaking by analyzing tilt series. Preliminary results from this study have failed to detect any significant change in register between successive molecules in a direction perpendicular to the plane of the sheet and so indicate that the true value of the pitch is close to 14.1 nm.

In addition to showing the density modulation due to the coiled-coil, the reconstructed image showed that coiled-coils in adjacent molecules across the sheet were staggered by a quarter pitch. This difference between adjacent molecules resulted in there being a glide plane parallel to the molecules' axis and so was consistent with the absence of an equatorial reflection at 3.9 nm in optical and electron diffraction patterns. There was also a pronounced striation perpendicular to the molecules' axes. This striation was probably related to variations in thickness due to the molecular length not being a multiple of the axial translation. If the molecule was 61 nm long as indicated by shadowing, it would span ~4.3 axial repeats of 14.1 nm. Therefore, in projection, each repeat would contain four full coils plus an extra one over about a third of the repeat length, and so there would be a corresponding axial density modulation. There was also a fine axial modulation present corresponding to the 0,7 meridional reflection. This periodicity probably represented some fine structure of the molecule, and, as it was at a spacing of 14.1/7

Table I. Fourier Data Obtained by Averaging Six Sets of Reflections

Miller indices			
h	k	Amplitude	Phase
		Arbitrary units	*Degrees*
−1	2	31	172
−1	4	6	5
0	1	30	−173
0	3	11	1
0	7	15	122
1	2	31	−161
1	4	5	36
2	0	104	0
2	1	12	55

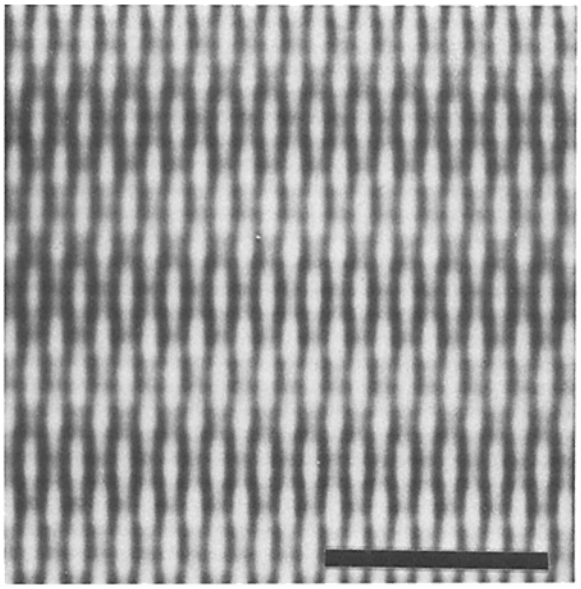

Figure 12. Reconstructed image of the top sheet of a negatively stained long S-2 tube (protein is white and stain dark). The image was produced by Fourier inversion of data deriving from six sets of reflections (Table I). The tube axis is horizontal. We interpret the prominent striations running perpendicular to the tube axis (that is, running vertically in this figure) as superimposed long S-2 molecules and the pronounced modulation along each striation as deriving from the coiled-coil as illustrated in Fig. 13. Note that coiled-coils in adjacent molecules are staggered by a quarter pitch. Bar, 20 nm.

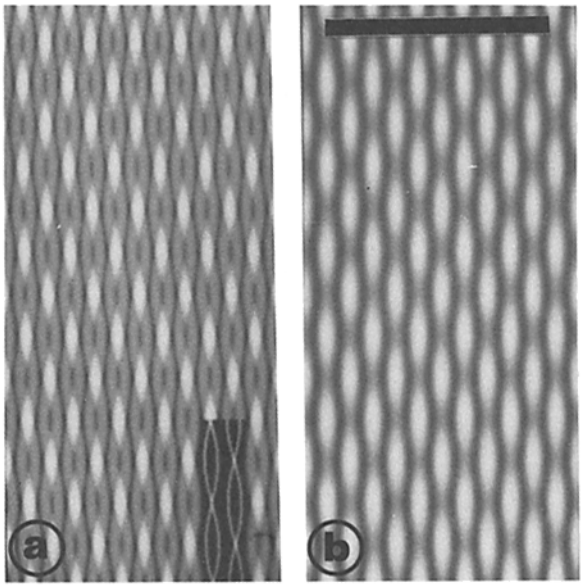

Figure 13. Schematic representation of the arrangement of coiled-coils seen in the projection of a negatively stained sheet (tube axis vertical). (*a*) The projected density due to an array of coiled-coils with pitch at 14.1 nm and lateral spacing at 1.9 nm. Each coiled-coil is modeled by two 1.1-nm diameter cylinders (representing α-helices; see Fraser and MacRae, 1973). The coils in adjacent molecules are staggered by a quarter pitch. (*Inset, bottom*) The path taken by the center of each α-helix. Because the coiled-coils in this arrangement are tightly packed, the array generally has an almost uniform density, except where the two α-helices in a coil cross over when the density doubles. There is also a very fine dark gap between coils. Consequently, the pattern produced is one of light areas (corresponding to the crossovers) on an almost uniform background. (*b*) The same image but at a resolution of 1.9 nm corresponding to the filtered image (Fig. 12). At this resolution, the fine dark lines between coils cannot be resolved, but the pattern of light areas corresponding to the crossovers of the α-helices remains. This pattern of light areas closely resembles the pattern seen in the image reconstructed from electron micrograph Fourier data (Fig. 12) and so indicates that the coiled-coils are arranged as illustrated in *a*. Bar, 20 nm.

nm, it may have been related to the periodicities in the myosin sequence that have a period of 28 residues (McLachlan and Karn, 1982, 1983). If the 28 residue periodicity in adjacent molecules was out of phase, as proposed by McLachlan and Karn (1982, 1983), then the first overtone should be absent (due to destructive interference) but the second overtone should remain. As noted by McLachlan and Karn (1982, 1983), 14.3 nm corresponds to 28 × 7/2 residues and so the second overtone of this period would occur at 14.3nm/7 or the seventh order of the axial repeat.

Discussion

Molecular Positions in the Crystalline Tube Wall

It is clear from the reconstructed image of the single side of the crystalline tube (Fig. 12) that the long S-2 molecules have two different orientations relative to their nearest neighbors. The first, which is apparent from simple inspection of Fig. 12, is that the nearest neighbors laterally (that is, in a direction in the plane of the sheet and circumferentially in a tube) are staggered by an odd number of coiled-coil quarter pitches, as illustrated in Fig. 13. This sort of interaction between coiled-coils is that proposed by Rudall (1956) on the basis of model studies, and also by Elliott and Bennett (1984) for the packing of paramyosin molecules within the very broad thick filaments from molluscan muscle. Although the present study does not directly establish the molecular arrangement in a direction perpendicular to the plane of the layer (that is, radially in the tube) it is clear from the thickness of the wall that there must be a number of molecules superimposed in this direction, and, since the coiled-coil pattern is quite clear after this superposition, it follows that consecutive molecules in a radial direction must be staggered by an integral number of half pitches (that is, 0, 7.2, 14.3.... nm). This is not the arrangement originally proposed by Rudall (1956), but is the arrangement deduced by Longley (1975) from a detailed model-building study of the way in which coiled-coils interact.

Since the thickness of the crystalline tubes is obviously limited in a radial direction (that is, perpendicular to the plane of the flattened tube observed by electron microscopy), the tube was probably not formed by a simple stacking of sheets of molecules. There would seem to be no obvious reason for a stack of sheets to be limited to a particular thickness, and instead one would expect a series of quantized thicknesses (here in steps of ~2 nm corresponding to the diameter of a coiled-coil) as seen, for example, in crystals (Dickson et al., 1978). One way in which the radial thickness of the tube could be limited would be if the molecules were

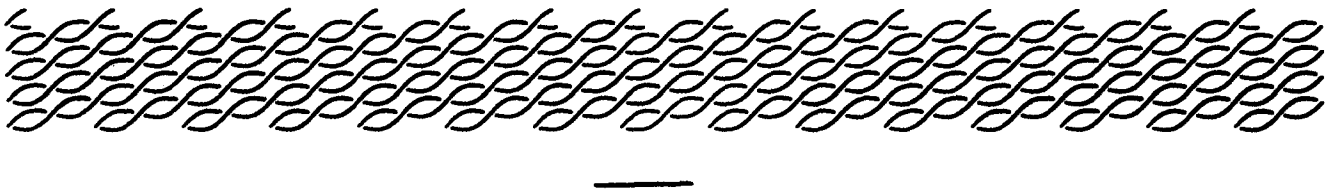

Figure 14. Illustration of a probable packing of long S-2 molecules within a sheet. Note that because of the small scale of each coiled-coil, the α-helical chains have been represented by a single continuous line rather than as a cylinder as in Fig. 13 *a*. The view shown here corresponds to a section through a single sheet perpendicular to the plane of the sheet and parallel to the molecules' axes and so illustrates the arrangement of successive molecules in a circumferential direction. Thus, in contrast to other figures in this article, the tube axis is directed out of the plane of the page. Molecules are oriented so that their NH_2 terminus protrudes from one side of the sheet and the COOH-terminus protrudes from the other. Successive molecules are staggered axially by 14.3 nm (one coiled-coil pitch) so that their coiled-coils are in register. This would account for the clarity of the coiled-coil modulation in projection and also for the series of striations 14 nm apart seen on the surface of the sheet by shadowing. A molecular length of 61 nm would give a thickness of ~8 nm and would generally correspond to four molecules being superimposed in a radial direction in the tube (that is, perpendicular to the plane of the sheet or vertically in this diagram). Because the molecular length is unlikely to be an integral number of half pitches, the ends of the molecules are different and this could give rise to a difference in appearance of the two faces of the tube. The scale bar is 14.1 nm but is only correct for measurements in the plane of the tube. To aid interpretation, dimensions have been exaggerated in a vertical direction.

slanted, as illustrated schematically in Fig. 14, so that each molecule traversed the entire radial thickness of the tube wall. The thickness of the tube would then be determined by the molecular length of long S-2. Measurements of the molecular length and the radial thickness of the tube wall were consistent with this hypothesis. Thus, if successive molecules were staggered by 14.3 nm as illustrated in Fig. 14, a molecular length of 61 nm would imply a radial thickness of ~8 nm, which is in good agreement with the value determined by low angle shadowing (Figs. 2 and 3). A stagger of this order would also be consistent with the 14-nm repeat in the direction of the molecular axes seen in shadowed images (Fig. 3) and transforms of negatively stained material (Fig. 5 and Table I). There would also be a slight foreshortening of the apparent coiled-coil pitch in projection but, in this model, the true value would be <1% greater than the value in projection.

The precise relationship between adjacent molecules across a sheet is not completely specified by the projection structure we have analyzed here because, although it is clear that the coiled-coils of these molecules must be staggered by an odd number of quarter pitches, neither their axial stagger nor their relative position radially in the tube (that is, perpendicular to the sheet) has been established. Thus, adjacent molecules could have the same radial position (giving a tetragonal unit cell in cross section), or, by analogy with Longley's (1975) modeling work and the molecular structure of paramyosin in thick filaments (Elliott and Bennett, 1984), they could be staggered by ~1 nm in this direction to give a body-centered lattice. This point can only be resolved by using tilt series to produce a three-dimensional reconstruction of the tube, and we are presently undertaking such a study.

It was not completely certain whether the molecules in the sheet were arranged parallel or antiparallel, since the positive staining pattern, which is usually used to establish this point in fibrous aggregates (e.g., Caspar et al., 1969), was very weak. There were, however, a number of indications that the molecules were all arranged with the same polarity. For example, there was a suggestion for shadowed material (Fig. 3) that the inner and outer surfaces of the tube could have been slightly different, which would be consistent with a polar organization. Another indication that the molecules may all have the same polarity was that, in a tube with a finite wall thickness, the outer circumference was greater than the inner. Since the winding of the sheets into tubes took place so readily and, moreover, always had the same hand, it seems likely that there must be some systematic difference between the inner and outer faces. This could occur in a structure such as that illustrated in Fig. 14 only if the long S-2 molecules were arranged in a polar manner, since with an antiparallel arrangement both faces would be identical. One way in which difference could arise between the different ends of long S-2 molecules is if the "hinge" region were to have a slightly different (and possibly more bulky) structure (see Harrington and Rodgers, 1985). Selective labeling at thiol residues, analogous to that achieved with tropomyosin (Stewart, 1975; Stewart and Diakiw, 1978; Stewart and Lepault, 1983) might be useful in establishing the polarity of the molecules in the sheets, but the lack of sequence data for chicken rod limits the potential usefulness of such an approach.

Coiled-Coil Pitch

The reconstructed image of a single side of a crystalline tube of long S-2 (Fig. 12) shows a clear density modulation, due to the coiled-coil structure of the molecule, and this appears to be the first instance where this has been seen by electron microscopy. This image established that the pitch of the long S-2 coiled-coil in these aggregates was close to the axial repeat of the unit cell, which was measured as 14.1 nm in projection. This probably corresponds to the prominent 14.3-nm repeat seen in muscle thick filaments (Huxley and Brown, 1967) and in many rod fragment paracrystals. Although the present results do not unequivocally establish that the LMM portion of myosin rod (the portion that interacts to form the thick filament shaft) has a coiled-coil pitch of 14.3 nm, they do make it likely that this is so, since detailed analysis of the sequence of myosin rod has indicated little difference between the S-2 and LMM portions (McLachlan and Karn, 1982, 1983) in that their amino-acid compositions are very similar and periodic dispositions of charged residues (with a repeat of 28) and hydrophobic residues (with a repeat of 7) are present in each. However, some caution

may be required in extrapolating this value to the myosin rods in muscle thick filaments and myosin aggregates in nonmuscle systems. It is possible that the coiled-coil pitch could be influenced by local packing considerations, as the torsional rigidity of a coiled-coil is probably not high.

The value of the S-2 coiled-coil pitch appears to be only slightly different from that of tropomyosin, which seems to be 13.7 nm (Stewart and McLachlan, 1975; Phillips et al. 1986). It is also within the range of 14–18 nm suggested for paramyosin, a coiled-coil protein similar to the myosin rod and which forms a major constituent of the shaft of many nonvertebrate myosin thick filaments (Cohen and Holmes, 1963; Elliot and Bennett, 1984; Elliot and Lowy, 1970; Elliott et al., 1968). (The x-ray diffraction studies were necessarily slightly imprecise because they relied on measuring the axial spacing of the second layer line of the coiled-coil transform, which was usually somewhat broad and, more importantly, was superimposed on a sloping background deriving from the equator of the x-ray patterns.) Furthermore, since the myosin rod sequence has a distinctive periodicity at 28 residues (and 28/3 and 28/10) that is also found in the sequences of keratins (McLachlan, 1978) and intermediate filaments (McLachlan and Stewart, 1982; Parry and Fraser, 1986), it seems possible that these coiled-coil proteins may have a similar pitch and assemble in a manner analogous to myosin rod.

Nature of Molecular Interactions

McLachlan and Karn (1982, 1983) and Parry (1981) showed that the myosin rod amino acid sequence has marked periodicities in its charged residues at frequencies of 28, 28/3, and 28/10 residues. Furthermore, they proposed that the molecules would interact in such a way as to neutralize the charge periodicity, which would occur with axial staggers between molecules of an odd multiple of 28/2 residues (for the fundamental component), which corresponds to odd multiples of ~2.1 nm. The most likely of these was thought to be 14.3 nm (McLachlan and Karn, 1982, 1983), corresponding to 7 × 28/2 residues. Moreover, structural repeats corresponding to this length are prominent in thick filaments (Huxley and Brown, 1967) and in paracrystal of myosin rod and its fragments (Bennett, 1976, 1981; Chowrashi and Pepe, 1977; Katsura and Noda, 1973; Safer and Pepe, 1979; Yagi and Offer, 1981). The stagger of 14.3 nm that we have inferred between molecules in a circumferential direction in the tube (i.e., along the molecules' axes) was clearly consistent with this, as was the axial periodicity corresponding to the seventh order of the 14.1-nm axial repeat. The weak positive staining pattern observed (Fig. 9) would also be consistent with this sort of interaction between molecules, because, by analogy with tropomyosin paracrystals (Stewart, 1981), charge complementation would probably greatly reduce specific attachment of uranyl ions to acidic residues in the sequence that formed salt bridges with basic residues.

The nature of the interaction between molecules staggered by an odd number of quarter pitches is less clear, but most possibilities do not seem consistent with the sort of charge complementation seen with a stagger of 14.3 nm. Instead of complementation of zones of positive and negative charge, it could be that, between molecules staggered by an odd number of quarter pitches, zones of the same charge are opposite one another and are linked by the divalent cations used to form the crystals, as proposed, for example, in tropomyosin magnesium paracrystals (Stewart, 1981). Alternatively, it could be that complementation of the 28/3 and 28/10 periodicities is involved rather than the fundamental 28 residue periodicity. Thus, if the 28/3 and 28/10 periodicities derived from a repeat at ~28/3.3 residues, staggering molecules by odd multiples of 28/6.6 residues could complement this repeat. A quarter pitch stagger would correspond to ~25 residues, which is close to 6 × 28/6.6.

Implications for Myosin-containing Filaments and Other Coiled-Coil Structures

Although long S-2 is probably not a major constituent of muscle thick filament shafts, the similarity of the diffraction patterns of a single layer (Figs. 5, 6, and 7) to those from molluscan muscle (Cohen and Holmes, 1963; Elliott et al., 1968; Elliott and Lowy, 1970; Elliot and Bennett, 1984) indicates that packing seen in the crystalline long S-2 tubes has direct biological relevance and probably closely resembles that seen in the paramyosin core of these filaments. The arrangement seen in Fig. 12, for example, is easily incorporated into Elliott and Bennett's (1984) model for the paramyosin core of molluscan thick filaments and also agrees closely with Longley's (1975) modeling. However, vertebrate skeletal muscle thick filaments seem to be constructed from units larger than a single molecule (Maw and Rowe, 1979; Pepe et al., 1981; Stewart et al., 1981*a*) and this seems to also be true for thick filaments from some other types of muscle (Wray, 1979). Consequently, the detailed molecular packing in these systems is probably not exactly the same as seen in the crystalline long S-2 sheets.

One feature of a 14.3-nm coiled-coil pitch is that the axial translation between parallel molecules in muscle thick filaments is almost certainly equal to, or is an integral multiple of, this distance. Consequently, the periodicity in the rod amino-acid sequence would be matched by a periodicity in the three-dimensional structure of the molecule. This could have important consequences for the structure of both muscle thick filaments and myosin aggregates in nonmuscle cells. It is, moreover, probably significant that there are clearly two types of interaction between coiled-coils in long S-2 tubes. This observation contrasts with computer analyses of charge interactions between myosin rods, which have tended to assume only one type of interaction, along the lines of early models for the arrangement of myosin tails in muscle thick filaments (Squire, 1973). More recent studies (Maw and Rowe, 1979; Pepe et al., 1981; Squire, 1981; Stewart and Kensler, 1986; Stewart et al., 1981*a*) have suggested that not all myosin molecules in these filaments are in equivalent environments, possibly as a result of assembling into subfilaments. It may therefore be rewarding to reexamine the myosin sequence data from this perspective.

The sorts of molecular interaction seen here may also be relevant to other aggregates of coiled-coil proteins. Although these interactions do not seem to be directly paralleled in crystals of tropomyosin (Phillips et al., 1986; Stewart, 1984) they may be of some significance for intermediate filaments and related structures. Thus, intermediate filament proteins (including α-keratins) have periodicities in their charged residues based on 28, 28/3, and 28/10 residues (McLachlan, 1978; McLachlan and Stewart, 1982; Parry and Fraser, 1986) that closely resemble those found in myosin rod (McLachlan

and Karn, 1982; 1983). Furthermore, intermediate filaments are probably constructed from subfilaments (Aebi et al., 1983) that seem analogous to the subfilaments proposed in vertebrate skeletal muscle. Also, in each case, molecular dimers can be formed in solution under defined conditions (Harrington and Rogers, 1985; Quinlan et al., 1984). It therefore seems possible that intermediate filament proteins may assemble in ways similar to myosin. Thus, the sorts of interactions observed in long S-2 crystalline tubes may be an example of a general form of interaction between coiled-coil proteins. Furthermore, our results raise the possibility that intermediate filament proteins could have a similar pitch to that of the myosin rod.

We are most grateful to our colleagues in Cambridge, in particular to Hugh Huxley and Richard Henderson, for many helpful and constructive criticisms and comments. We also thank Sue Whytock for performing the shadowing experiments and Judy Smith, Richard Henderson, and Terry Horsnell for computer programs.

Received for publication 11 October 1986, and in revised form 9 February 1987.

References

Aebi, U., W. E. Fowler, P. Rew, and T.-T. Sun. 1983. The fibrillar substructure of keratin filaments unravelled. *J. Cell Biol.* 97:1131–1143.

Aebi, U., W. E. Fowler, E. L. Buhle, and P. R. Smith. 1984. Electron microscopy and image processing applied to the study of protein structure and protein-protein interactions. *J. Ultrastruct. Res.* 88:143–176.

Bennett, P. M. 1976. Molecular packing in light meromyosin paracrystals. *Proc. VI Eur. Cong. Electron Microsc.* Vol. II:517–519.

Bennett, P. M. 1981. The structure of spindle-shaped paracrystals of light meromyosin. *J. Mol. Biol.* 146:201–221.

Brisson, A., and P. N. T. Unwin. 1984. Tubular crystals of acetylcholine receptors. *J. Cell Biol.* 99:1202–1211.

Caspar, D. L. D., C. Cohen, and W. Longley. 1969. Tropomyosin crystal structure, polymorphism and molecular interactions. *J. Mol. Biol.* 41: 87–107.

Castellani, L., P. Vibert, and C. Cohen. 1983. Structure of myosin: paramyosin filaments from a molluscan smooth muscle. *J. Mol. Biol.* 167:853–872.

Chowrashi, P. K., and F. A. Pepe. 1977. Light meromyosin paracrystal formation. *J. Cell Biol.* 74:136–152.

Cohen, C., and K. C. Holmes. 1963. X-ray diffraction evidence for α-helical coiled-coils in native muscle. *J. Mol. Biol.* 6:423–432.

Cohen, C., and D. A. D. Parry. 1986. Alpha-helical coiled-coils—a widespread motif in proteins. *Trends Biochem. Sci.* 11:245–248.

Crick, F. H. C. 1953. The Fourier transform of a coiled-coil. *Acta Crystallogr. Sect. B Struct. Crystallogr. Cryst. Chem.* 6:685–689.

Crowther, R. A., R. Craig, and R. Padron. 1985. Arrangement of the heads of myosin in relaxed thick filaments from tarantula muscle. *J. Mol. Biol.* 184:429–439.

DeRosier, D. J., and P. M. Moore. 1970. Reconstruction of three-dimensional images from electron micrographs of structures with helical symmetry. *J. Mol. Biol.* 52:355–369.

Dickson, M. R., M. Stewart, D. E. Hawley, and C. A. Marsh. 1978. An electron microscope study of beta-glucuronidase crystals. *Biochem. J.* 181:1–5.

Elliott, A., and P. M. Bennett. 1984. Molecular organisation of paramyosin in the core of molluscan thick filaments. *J. Mol. Biol.* 176:477–493.

Elliott, A., and J. Lowy. 1970. A model for the coarse structure of paramyosin filaments. *J. Mol. Biol.* 53:181–203.

Elliott, A., J. Lowy, D. A. D. Parry, and P. J. Vibert. 1968. Puzzle of the coiled-coils in the α-protein paramyosin. *Nature (Lond.).* 218:656–659.

Fraser, R. D. B., and MacRae, T. P. 1973. Conformation in Fibrous Proteins. Academic Press, Inc., New York. 628 pp.

Harrington, W. F., and M. E. Rodgers. 1985. Myosin. *Annu. Rev. Biochem.* 53:35–73.

Henry, N. F. M., and K. Lonsdale, editors. 1969. International Tables for X-ray Crystallography. Vol I. Kynoch Press, Birmingham, AL. 58–62.

Huxley, H. E., and W. F. Brown. 1967. The low-angle X-ray diagram of vertebrate skeletal muscle and its behaviour during contraction and rigor. *J. Mol. Biol.* 30:383–434.

Katsura, I., and H. Noda. 1973. Structure and polymorphism of light meromyosin aggregates. *J. Biochem. (Tokyo).* 73:257–268.

Kensler, R. W., and M. Stewart. 1983. Frog skeletal muscle thick filaments are three-stranded. *J. Cell Biol.* 96:1797–1802.

Kensler, R. W., and M. Stewart. 1986. An ultrastructural study of cross-bridge arrangement in the frog thigh muscle thick filament. *Biophys. J.* 49:343–351.

Klug, A., and D. J. DeRosier. 1966. Optical filtering of electron micrographs: reconstruction of one-sided images. *Nature (Lond.).* 212:29–32.

Laemmli, U. 1970. Cleavage of structural proteins during the assembly of the head of bacteriophage T4. *Nature (Lond.).* 227:680–685.

Longley, W. 1975. The packing of double helices. *J. Mol. Biol.* 93:111–115.

McLachlan, A. D. 1978. Coiled-coil formation and sequence regularities in the helical regions of α-keratin. *J. Mol. Biol.* 124:297–304.

McLachlan, A. D., and J. Karn. 1982. Periodic charge distributions in the myosin rod amino-acid sequence match crossbridge spacings in muscle. *Nature (Lond.).* 299:226–231.

McLachlan, A. D., and J. Karn. 1983. Periodic features of the amino acid sequence of nematode myosin rod. *J. Mol. Biol.* 164:605–626.

McLachlan, A. D., and M. Stewart. 1982. Periodic charge distribution in the intermediate filament proteins desmin and vimentin. *J. Mol. Biol.* 162:693–698.

Maw, M., and A. Rowe. 1980. Fraying of A-filament into three subfilaments. *Nature (Lond.).* 286:412–414.

Namba, K., and G. Stubbs. 1986. Structure of tobacco mosaic virus at 3.6A resolution: implications for assembly. *Science (Wash. DC).* 231:1401–1406.

Parry, D. A. D. 1981. Structure of rabbit skeletal myosin. Analysis of the amino acid sequences of two fragments from the rod region. *J. Mol. Biol.* 153:459–464.

Parry, D. A. D., and Fraser, R. D. B. 1986. Intermediate filament structure: 1. Analysis of IF protein sequence data. *Int. J. Biol. Macromol.* 7:203–214.

Pepe, F. A., F. A. Ashton, and M. Stewart. 1981. The myosin filament VII. Changes in internal structure along the filament. *J. Mol. Biol.* 145:421–440.

Phillips, G. N., J. P. Fillers, and C. Cohen. 1986. Tropomyosin crystal structure and muscle regulation. *J. Mol. Biol.* 192:111–131.

Quinlan, R. A., J. A. Cohlberg, D. L. Schiller, M. Hatzfeld, and W. W. Franke. 1984. Heterotypic tetramer (A_2D_2) complexes of nonepidermal keratins isolated from cytoskeletons of hepatocytes and hepatoma cells. *J. Mol. Biol.* 178:365–388.

Rudall, K. M. 1956. Protein ribbons and sheets. *Lect. Sci. Basis Med.* 5:217–230.

Safer, D., and F. A. Pepe. 1979. Axial packing in light meromyosin paracrystals. *J. Mol. Biol.* 136:343–358.

Squire, J. M. 1973. General model for myosin filament structure. III. Molecular packing arrangement in myosin filaments. *J. Mol. Biol.* 77:291–323.

Squire, J. M. 1981. The Structural Basis of Muscle Contraction. Plenum Press. London.

Stafford, W. F. 1985. Effect of various anions on the stability of the coiled-coil of skeletal myosin. *Biochemistry.* 24:3314–3321.

Stewart, M. 1975. Location of the troponin binding site on tropomyosin. *Proc. R. Soc. Lond. B Biol. Sci.* 190:257–266.

Stewart, M. 1981. Structure of α-tropomyosin magnesium paracrystals. II: simulation of staining patterns from the sequence and some observations on the mechanism of positive staining. *J. Mol. Biol.* 148:411–425.

Stewart, M. 1982. Chain register in myosin rod. *FEBS (Fed. Eur. Biochem. Soc.) Lett.* 140:210–212.

Stewart, M. 1984. Crystalline sheets of tropomyosin. *J. Mol. Biol.* 174:231–238.

Stewart, M. 1986. Computer analysis of ordered microbiological objects. *In* Ultrastructure Techniques for Microorganisms. H. C. Aldrich and W. J. Todd, editors. Plenum Publishing Corp., New York. 333–364.

Stewart, M., and T. J. Beveridge. 1980. Structure of the regular surface layer of *Sporosarcina ureae. J. Bacteriol.* 142:302–309.

Stewart, M., and Diakiw, V. 1978. Electron microscopic location of protein thiol groups. *Nature (Lond.).* 274:184–186.

Stewart, M., and P. Edwards. 1984. Length of myosin rod and its proteolytic fragments determined by electron microscopy. *FEBS (Fed. Eur. Biochem. Soc.) Lett.* 168:75–78.

Stewart, M., and R. W. Kensler. 1986. The arrangement of myosin heads in relaxed thick filaments from frog skeletal muscle. *J. Mol. Biol.* 192:831–851.

Stewart, M., and J. Lepault. 1983. Cryo electron microscopy of tropomyosin magnesium paracrystals. *J. Microsc. (Oxf.).* 138:53–60.

Stewart, M., and A. D. McLachlan. 1975. 14 actin binding sites on tropomyosin? *Nature (Lond.).* 257:331–333.

Stewart, M., F. A. Ashton, R. Lieberson, and F. A Pepe. 1981*a*. The myosin filament IX. Determination of subfilament position by computer image processing. *J. Mol. Biol.* 153:381–392.

Stewart, M., R. W. Kensler, and R. J. C. Levine. 1981*b*. Structure of *Limulus* telson muscle thick filaments. *J. Mol. Biol.* 153:781–790.

Stewart, M., T. J. Beveridge, and G. D. Sprott. 1985*a*. Crystalline order to high resolution in the sheath of *Methanospirillum hungatei. J. Mol. Biol.* 183:509–515.

Stewart, M. R. W. Kensler, and R. J. C. Levine. 1985*b*. Three-dimensional reconstruction of thick filaments from *Limulus* and scorpion muscle. *J. Cell Biol.* 101:402–411.

Sutoh, K., K. Sutoh, T. Karr, and W. F. Harrington. 1978. Isolation and physico-chemical characterisation of a high molecular weight subfragment-2 of myosin. *J. Mol. Biol.* 126:1–22.

Ueno, H., M. E. Rodgers, and W. F. Harrington. 1983. Self-association of a high molecular weight subfragment-2 of myosin induced by divalent cations. *J. Mol. Biol.* 168:207–228.

Valentine, R. C., B. M. Shapiro, and E. R. Stadtman. 1968. Regulation of glutamine synthetase XII: electron microscopy of the enzyme from *E. coli*. *Biochemistry*. 7:2143–2152.

Vibert, P., and R. Craig. 1983. Electron microscopy and image analysis of myosin filaments from scallop striated muscle. *J. Mol. Biol.* 165:303–320.

Walzthony, D., H. M. Eppenberger, H. Ueno, W. F. Harrington, and T. Wallimann. 1986. Melting of myosin rod as revealed by electron microscopy. II. Effects of temperature and pH on length and stability of myosin rod and its fragments. *Eur. J. Cell Biol.* 41:38–43.

Weeds, A. G., and B. Pope. 1977. Studies on the chymotryptic digestion of myosin. Effects of divalent cations on proteolytic susceptibility. *J. Mol. Biol.* 111:129–157.

Wray, J. S. 1979. Structure of the backbone of myofilaments in muscle. *Nature (Lond.)*. 277:37–40.

Yagi, N., and G. Offer. 1981. X-ray diffraction and electron microscopy of a light meromyosin tactoid. *J. Mol. Biol.* 151:467–490.

Yanagida, M., D. J. DeRosier, and A. Klug. 1972. The structure of tubular variants of the head of bacteriophage T4. *J. Mol. Biol.* 65:489–499.